Article

AuPt Nanoparticles Clusters on MWCNTs with Enhanced Electrocatalytic Activity for Methanol Oxidation

Changzheng Wang [1], **Fengnan Yang [1]**, **Li Gao [2]**, **Shoufang Xu [3],***, **Louzhen Fan [2],***, **Tao Guo [1]**, **Yongfeng Liu [1]**, **Lian Zhou [1]** and **Yang Zhang [4],***

[1] Beijing Key Laboratory of Functional Materials for Building Structure and Environment Remediation, Beijing University of Civil Engineering and Architecture, Beijing 100044, China

[2] Department of Chemistry, Beijing Normal University, Beijing 100875, China

[3] School of Materials Science and Engineering, Linyi University, Linyi 276005, China

[4] Beijing Institute of Nanoenergy and Nanosystems, Chinese Academy of Sciences, Beijing 100083, China

* Correspondence: xshfang1981@163.com (S.X.); lzfan@bnu.edu.cn (L.F.); zhangyang0037@sina.com (Y.Z.); Tel.: +86-539-7258661 (S.X.); +86-10-58805372 (L.F.); +86-10-82854792 (Y.Z.)

check for updates

Abstract: AuPt nanoparticles clusters (NPCs) were electrodeposited on multiwalled carbon nanotubes (MWCNTs). The as-prepared AuPt NPCs@MWCNTs nanocomposites exhibited considerably enhanced electrocatalytic activity than Pt NPs@MWCNTs for methanol oxidation in acid medium. In comparison with Pt NPs@MWCNTs, a remarkable resistance to CO poisoning and a higher I_f/I_b value (the ratio of the forward scan oxidation peak current (I_f) and reverse scan oxidation peak current (I_b)) was achieved by AuPt NPCs@MWCNTs electrocatalyst, which is attributable to the unique NPCs nanostructure with enlarged electrochemical active surface areas. These results demonstrated the potential of AuPt NPCs@MWCNTs, which can be considered as an efficient electrocatalyst for methanol oxidation in direct methanol fuel cells.

Keywords: AuPt nanoparticles clusters; MWCNTs; nanocomposites; electrocatalytic activity; methanol oxidation

1. Introduction

Methanol oxidation [1–11] is considered to be one of the environmental-friendly and sustainable source of energy, in which the methanol is supplied directly to the electrode where it is converted to carbon dioxide. In principle, methanol oxidation can directly convert the chemical energy of methanol into electrical energy, and the reaction products are mainly water and carbon dioxide. Recently, methanol oxidation has attracted great attention due to its simple structure, low energy consumption, high energy density, and limited cost [12,13].

Efficient electrocatalysts for methanol oxidation can improve the energy output efficiency and overall performance of the device as well as accelerate the electrode reaction and suppresses side reactions [14–16]. Because of its higher catalytic activity towards methanol oxidation and excellent corrosion resistance [17–22], Pt and its alloys with transition metals are the most effective electrocatalysts in terms of methanol oxidation. However, the large-scale applications of methanol oxidation have been considerably restricted by the high cost and low abundance of Pt and other noble-metal based electrocatalysts, and unsolved problems, such as Pt poisoning. Previous works [23] have indicated potential solutions to the current bottlenecks by enhancing dispersion of the nanostructured Pt on a suitable carrier and combining other metals with Pt by forming bimetallic or multi-metal electrocatalysts, respectively.

In recent years, the research of methanol oxidation as an electrocatalyst carrier for designing low-temperature fuel cells has attracted broad attention [24,25]. According to previous publications, the multiwalled carbon nanotubes (MWCNTs) have good conductivity, a higher specific surface area, a tunable surface function, and other unique physical and chemical properties. In fact, MWCNTs-supported electrocatalysts have demonstrated excellent electrocatalytic performance in comparison with carbon black in terms of methanol oxidation. Therefore, the networks of MWCNTs were employed as the carrier for loading and dispersing metal NPs' catalyst [26–29], which demonstrates improved electrocatalytic performance [30]. Haruta et al. [31–33] revealed that Au NPs have good catalytic activity for the electro-oxidation of carbon monoxide. Because of the interaction between a second metal and Pt, the electrocatalytic activities could be further promoted [34–39]. Recently, it was reported that Au-Pt catalyst could be synthesized by a convenient co-impregnation method. Furthermore, the synthesis of AuPt-based nanomaterials on MWCNTs is still deserving of further investigation into the performance of the methanol oxidation reaction. Taking advantage of the electrochemical technique, simple operation and high product purity can be achieved. In this work, we performed the electrochemical deposition method to prepare AuPt nanoparticles clusters on MWCNTs (NPCs@MWCNTs). Compared to Pt NPs@MWCNTs, we found that the AuPt NPCs@MWCNTs exhibited higher activity, which is promising as a candidate in enhancing the electrocatalytic activity toward methanol oxidation.

2. Results and Discussion

2.1. Materials Characterization

The morphology of AuPt NPCs on the surface of MWCNTs was investigated by scanning electron microscopy (SEM) characterization. Figure 1 shows SEM images of bare MWCNTs and AuPt NPCs@MWCNTs, which confirms the formation of AuPt NPCs@MWCNTs. The SEM characterizations reveal the as-received SEM image of MWCNTs with a smooth surface. Furthermore, the amount and size of AuPt NPCs can be tuned by increasing different electrodeposition times. As shown in Figure 1b, the size of AuPt NPs prepared by 1 minute electrodeposition was found to be a few nanometers, which dispersed on the surface of MWCNTs and formed 10 nm AuPt NPCs@MWCNTs nanocomposite. As the electrodeposition time was increased to 5 min, more AuPt NPs were found to form AuPt NPCs nanostructures with a size of 30–40 nm (see Figure 1c). When electrodeposition time was increased from 5 min to 10 min, we found that the formed AuPt NPCs further accumulated on the MWCNTs' surface. The size of as-synthesized AuPt NPCs was approximately 100 nm, which can be seen in Figure 1d. It can be observed that a large amount of aggregated AuPt NPCs coated the MWCNTs' surface.

Transmission electron microscopy (TEM) characterization was employed to investigate AuPt NPCs@MWCNTs. AuPt NPCs were found to disperse on the MWCNTs' surfaces by electrochemical deposition as described in the experimental section. The corresponding morphologies of the AuPt NPCs are shown in Figure 2a,b, respectively. Figure 2a shows the AuPt NPCs with a size of 10 nm anchored to MWCNTs, indicating the formation of AuPt NPCs@MWCNTs as a stable nanocomposite. As the electrodeposition time was increased to 5 min, more details can be found in Figure 2b, which unveil that the AuPt NPCs is about 30 nm–40 nm in size and serve as a self-assembly building block for NPCs. It should be pointed out that AuPt NPs with a largely exposed surface offers an additional advantage for electrocatalytic activities.
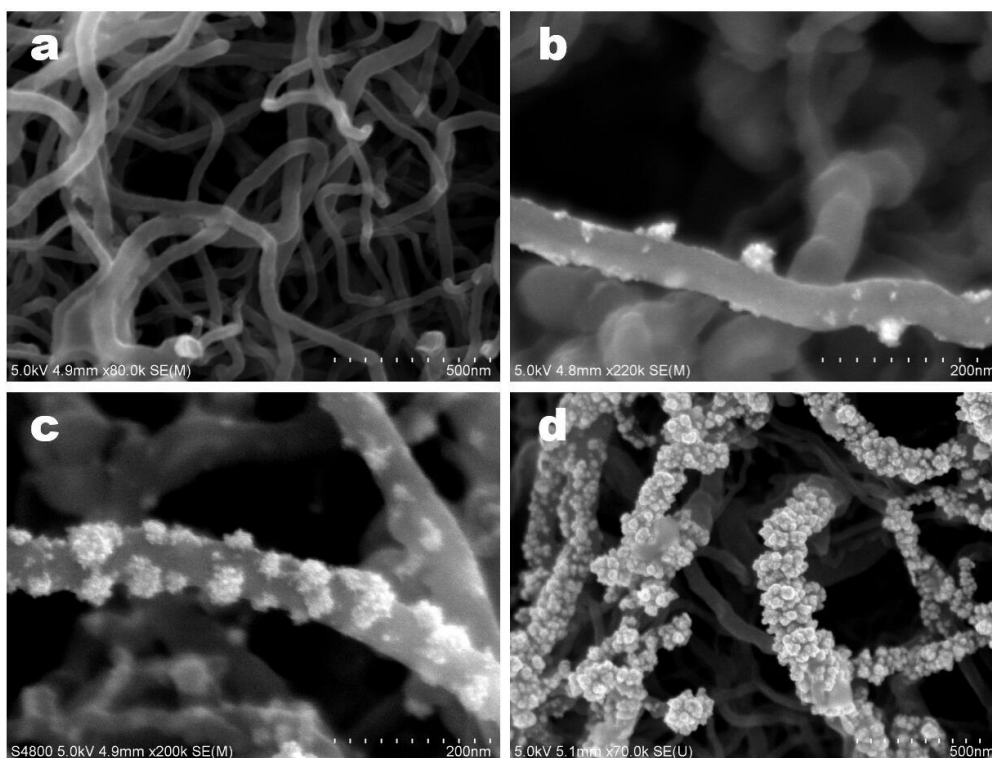
Figure 1. SEM images of (**a**) as-received MWCNTs and AuPt NPCs@MWCNTs synthesized with different electrodeposition times: (**b**) 1 min, (**c**) 5 min, and (**d**) 10 min.
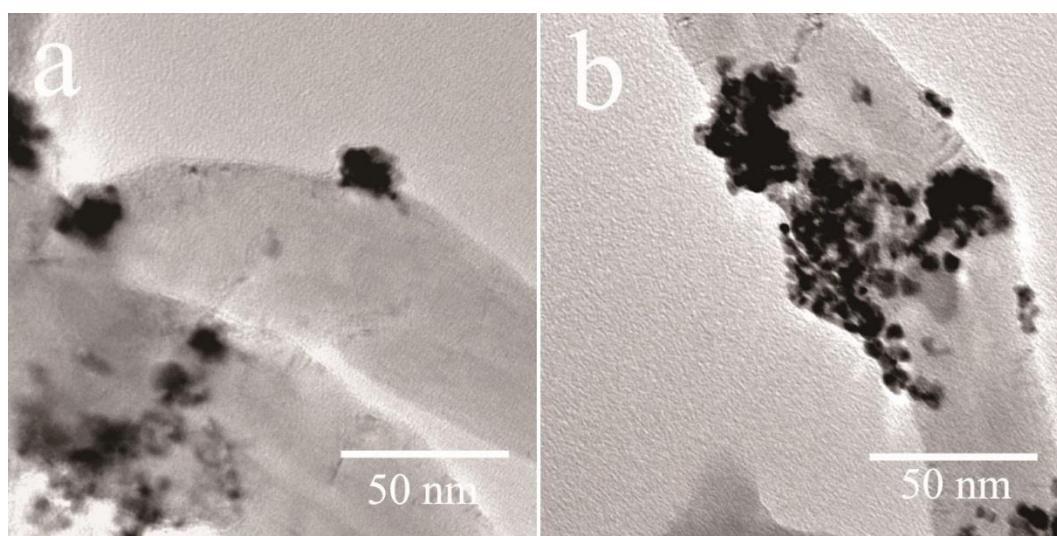
Figure 2. TEM images of AuPt NPCs@MWCNTs synthesized with different electrodeposition times: (**a**) 1 min and (**b**) 5 min.

Compared with the AuPt NPCs@MWCNTs nanocomposite, we performed the same technique to synthesize Pt NPs@MWCNTs. The typical SEM image of Pt NPs@MWCNTs is shown in Figure 3. The surface of MWCNTs is mostly covered by dispersed Pt NPs, which indicates that the addition of Au facilitates the formation of the AuPt NPCs.
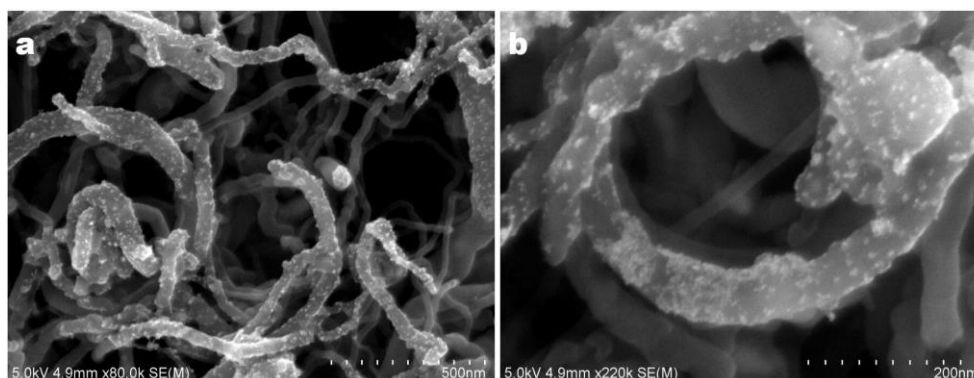
Figure 3. SEM image of Pt NPs@MWCNTs synthesized with (**a**) low and (**b**) high magnifications.

Figure 4a presents the X-ray diffraction (XRD) pattern of the as-prepared AuPt NPCs@MWCNTs. As shown in Figure 4a, the Au (111), (200), (220), (311), (222) and Pt (111), (200), (220), (311), (222) peaks provide evidence that crystalline AuPt NPs formed on the surface of MWCNTs. The diffraction peaks at 2θ = 38.9°, 45.2°, 65.9°, and 79.4° are consistent with the face-centered cubic (fcc) structure of Au (38.3°, 44.4°, 64.6°, and 77.5°) and Pt (39.8°, 46.2°, 67.4°, and 81.3°), respectively. The position of four characteristic signals can be indexed to the Au and Pt fcc crystal structure compared with the standard JCPDS card (No. 4-783). Based on our experimental results, the diffraction peaks of oxides of Au and Pt were not observed. It can be concluded that AuPt NPCs were prepared by forming bimetallic nanocomposite rather than the mixture of Au NPs@MWCNTs and Pt NPs@MWCNTs [40,41].
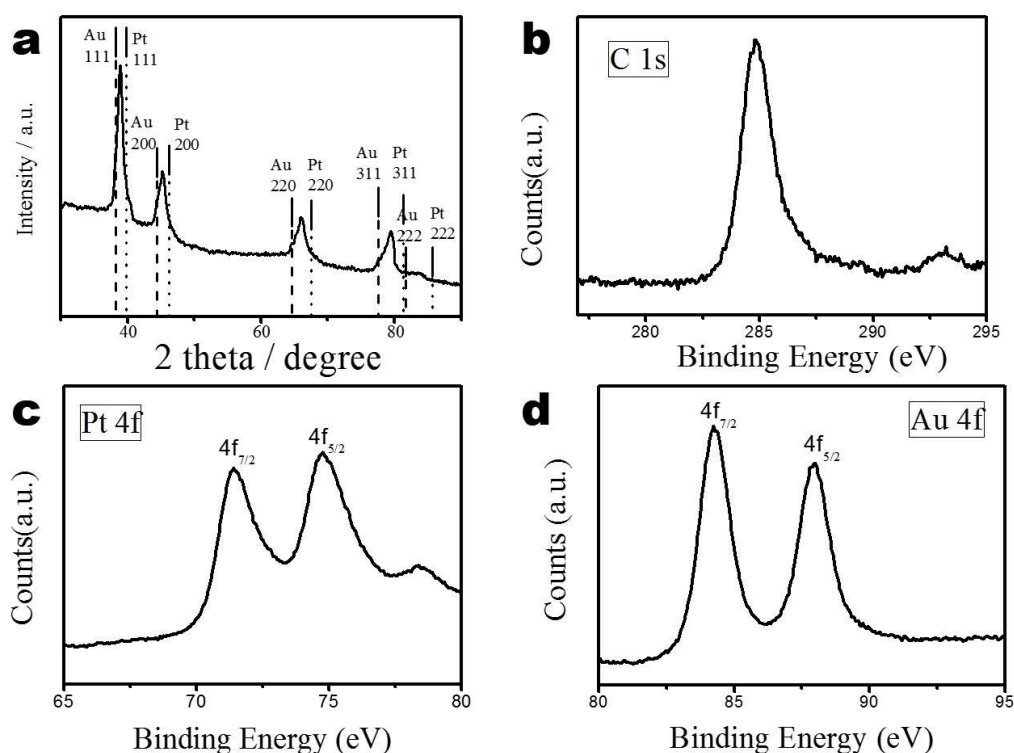
Figure 4. (**a**) XRD pattern of AuPt NPCs@MWCNTs, XPS spectra of AuPt NPCs@MWCNTs: (**b**) C1s, (**c**) Pt 4f, and (**d**) Au 4f.

The X-ray photoelectron spectroscopy (XPS) analyses of AuPt NPCs@MWCNTs were conducted as well, which are shown in Figure 4b–d. Figure 4b shows the XPS image of C1s, the binding energy for C1s peak was 284.6 eV corresponding to the C–C energy of the carbon nanotubes [42]. There was no oxygen peak in C1s' region, indicating no oxygen bond forming outside of MWCNTs [43]. Figure 4c

shows the XPS spectrum of Pt 4f, the peak of Pt $4f_{7/2}$ and Pt $4f_{5/2}$ was found at 71.4 and 74.8 eV. The XPS characterizations gave no signal of Pt^{2+} and Pt^{4+} (around 73.8 eV and 74.6 eV), which supported that alloyed Pt NPs were at a zero valence state. In addition, Figure 4d shows the XPS spectrum of Au 4f, which exhibits the typical peaks of Au $4f_{7/2}$ and Au $4f_{5/2}$ were found at 84.2 and 87.9 eV. According to previous reports [44], the binding energy of the Au component in AuPt NPs are zero valence as well. In comparison with Pt NPs@MWCNTs (Pt $4f_{7/2}$: 71.9 eV and Pt $4f_{5/2}$: 74.5 eV), the Pt $4f_{7/2}$ and $4f_{5/2}$ peaks of AuPt NPCs slightly shifted, which reveals the electron structure of Pt was changed due to the existence of the Au component.

2.2. Electrochemical Characterization and Activity

To explore the relationship of between morphology and electrocatalytic activity of AuPt NPCs@MWCNTs for methanol oxidation, the cyclic voltammograms of as-prepared samples were measured in the solution of 0.1 M Na_2SO_4 containing 2.0 M CH_3OH. As shown in Figure 5a, the current of methanol oxidation increases first and then decreases, which will be discussed in detail below. Because of the electrodeposition time of 1 min, only some AuPt NPs or a small amount of AuPt NPCs was deposited on the surface of MWCNTs and formed a nanocomposite. More importantly, the formation of AuPt NPCs efficiently increased the active center of Pt with an electrodeposition time of 5 min, which further facilitated the methanol oxidation reaction. However, the current of methanol oxidation decreased by further increasing the electrodeposition time to 10 min, which resulted from the accumulation of AuPt NPCs on the MWCNTs' surface. Indeed, the overgrowth of AuPt NPCs led to the reduction of the active sites of the electrocatalyst for methanol oxidation. Figure 5b presents the cyclic voltammograms of AuPt NPCs@MWCNTs and Pt NPs@MWCNTs in the 0.1 M H_2SO_4 solution with an electrodesiposition time of 5 min. Both of AuPt NPCs@MWCNTs and Pt NPs@MWCNTs have two pairs of hydrogen adsorption-desorption peaks between −0.25 and 0 V, which indicates both had electrocatalytic activity to hydrogen oxidation reduction. Compared to Pt NPs@MWCNTs, AuPt NPCs@MWCNTs demonstrate a larger hydrogen adsorption-desorption, reduction of oxygen, and oxidation peak current. Our result indicates that the addition of Au enhances the activity of Pt-based electrocatalysts and increases the utilization of Pt atoms on the nanocomposite surface. As discussed in SEM and TEM characterization, the AuPt NPCs on the surface of MWCNTs were composed of small NPs, which largely increase the electrochemical active surface areas (ECSAs). Based on the cyclic voltammograms of hydrogen desorption at the electrode surface (the first reduction peak corresponding to the reoxidation peak), the calculated ECSAs [45] of AuPt NPCs@MWCNTs was 72.23 m^2/g, while ECSAs of Pt NPs@MWCNTs was only 7.76 m^2/g. It can be concluded that the enhanced performance of methanol oxidation is attributed to the improved ECSAs, which resulted from the optimized nanostructure design.
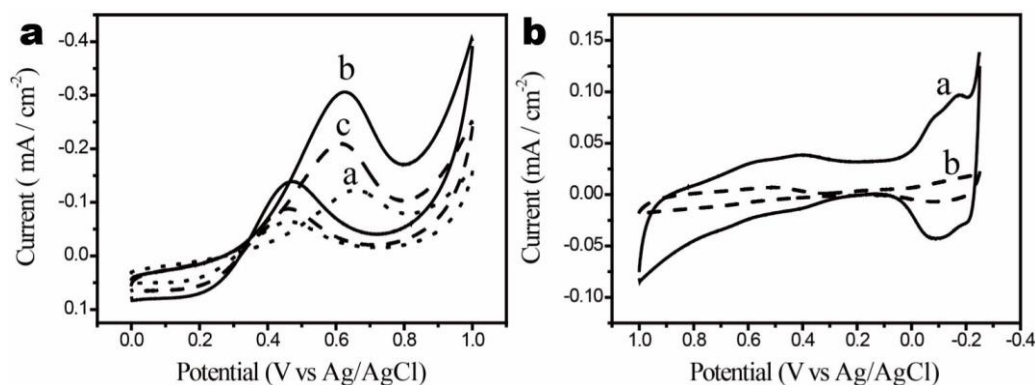
Figure 5. (**a**) Cyclic voltammograms of AuPt NPCs@MWCNTs nanocomposite synthesized at different electrodeposition times: (a) 1 min, (b) 5 min, (c) 10 min in 2.0 M CH_3OH and 0.1 M Na_2SO_4 solution. Scanning rate: 100 $mV \cdot s^{-1}$; (**b**) cyclic voltammograms of (a) AuPt NPCs@MWCNTs and (b) Pt NPs@MWCNTs in 0.1 M H_2SO_4 solution. Scanning rate is 100 $mV \cdot s^{-1}$.

Furthermore, the electrocatalytic performance of as-prepared AuPt NPCs@MWCNTs and Pt NPs@MWCNTs with the same electrodeposition time (5 min) were investigated in the acid condition (0.1 M H_2SO_4 solution containing 2.0 M CH_3OH). Both had electrocatalytic activity to the methanol oxidation reaction, a forward oxidation peak and a reverse oxidation peak can be clearly observed in the range of the 0 V to 1.0 V potential window (see Figure 6a). It should be mentioned that the dissociative adsorption of methanol produces a series of intermediate products, including bonded carbon monoxide, which poison the electrocatalyst Pt (existing in the form of Pt-CO). As the scanning potential increased, these intermediates were oxidized to generate CO_2, which were removed from the electrocatalyst surface. The corresponding cyclic voltammograms show a forward oxidation peak, which was employed to evaluate the performance of the electrocatalyst. In the reverse scan, there was methanol dissociative adsorption again at the previously mentioned active sites and a series of intermediate products. Therefore, the relevant reaction on the cyclic voltammogram was related to the peak in the reverse scan. It can be seen that the oxidation peak current in the forward scan of AuPt NPCs@MWCNTs was much higher than the current of Pt NPs@MWCNTs due to the addition of the Au component. The ratio of the forward scan oxidation peak current (I_f) and reverse scan oxidation peak current (I_b) can be employed to evaluate the endurance of carbonaceous intermediates' accumulation [46]. It is known that a higher I_f/I_b value indicates a better CO electrooxidation ability. Based on our experimental results, the I_f/I_b of AuPt NPCs@MWCNTs (2.4) was higher than the Pt NPs@MWCNTs (1.7). It illustrates that the most carbonaceous intermediate products were oxidized to CO_2 with the help of the Au component. The stability of AuPt NPCs@MWCNTs and Pt NPs@MWCNTs was tested in the same conditions. In Figure 6b, it can be found that the forward scanning peak currents decrease over the repeated test cycles, which can be explained as the intermediate products accumulating on the surface of electrocatalysts in a long period of continuous scanning. After 50 cycles, the above-mentioned two samples were placed in deionized water for 24 h and then taken out for repetition of the methanol oxidation reaction. The maximum value of the AuPt NPCs@MWCNTs and Pt NPs@MWCNTs forward scanning oxidation peaks were 81.3% and 31.7%, respectively. It can be interpreted that most of the carbonaceous intermediate products in the forward oxidation scanning were oxidized to CO_2 in the case of the AuPt NPCs@MWCNTs sample, which confirmed that the combination of Au and Pt can improve the Pt-based catalyst poisoned by the intermediates.
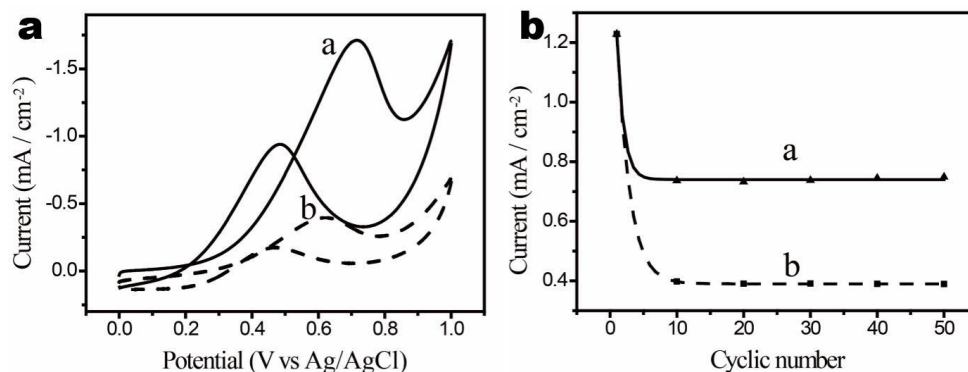
Figure 6. (**a**) Cyclic voltammograms of (a) AuPt NPCs@MWCNTs, and (b) Pt NPs@MWCNTs in the mixed solution of 2 M CH_3OH and 0.1 M H_2SO_4. Scanning rate is $100 mV \cdot s^{-1}$; (**b**) cycle stability of (a) AuPt NPCs@MWCNTs, (b) Pt NPs@MWCNTs electrodes in 0.1 M H_2SO_4 solution containing 2 M CH_3OH.

3. Materials and Methods

3.1. Materials

MWCNTs were purchased from Shenzhen Nanotech. Port. Co., Ltd (Shenzhen, China) and further purified prior for use by stirring in concentrated nitric acid for 12 h. Toluene ($C_6H_5CH_3$) (Park Co. Dublin, Ireland) was dried with Na and refluxed for 6 h before distillation and then stored in the presence of Na. Other reagents included deionized H_2O, K_2SO_4 (analytical reagent (AR), Nacalai Tesque, Inc. Kyoto, Japan), K_2PtCl_4 (99.9% Pt, General Research Institute for Nonferrous Metals, Beijing, China), H_2SO_4 (AR, BeiHua, Inc., Beijing, China), ethanol (CH_3CH_2OH) (AR, Chemical Reagent, Inc. Tianjin, China), and CH_3OH (anhydrous AR BeiHua, Inc., Beijing, China).

3.2. AuPt NPCs@MWCNTs Electrode Preparation

The conductive indium tin oxides (ITO) was cleaned in acetone and absolute alcohol solution for 15 min, respectively, before use, and finally dried in ambient conditions. 1 mg MWCNTs was dispersed in 10 mL toluene under ultrasound for 30 min, which formed $0.1 mg \cdot mL^{-1}$ suspensions. The MWCNTs-modified ITO electrodes (MWCNTs/ITO) were prepared by dipping 10 µL suspension on ITO electrodes and then were dried at room temperature. In this work, the electrochemical experiments were conducted in a three-electrode system. The working electrode was MWCNTs/ITO, a platinum wire (Pt) was used as a counter electrode, and a silver/silver chloride (Ag/AgCl) electrode was used as the reference electrode. The electrolyte was a mixed solution of 1 mM K_2PtCl_6 and 1mM $HAuCl_4$, and electrodepositing was performed under an overpotential of −0.3 V. Before the electrodeposition, MWCNTs/ITO electrodes were stored in a mixed solution of K_2PtCl_6 and $HAuCl_4$ for 12 h.

3.3. Pt NPs@MWCNTs Electrode Preparation

The Pt NPs@MWCNTs samples were prepared also by using the three-electrode system as well. The working electrode was MWCNTs/ITO, and a platinum wire and Ag/AgCl electrode was used as the counter electrode and the reference electrode, respectively. The electrolyte was 0.1 mM K_2PtCl_6 solution and electrodepositing processes were carried out under an overpotential of −0.6 V.

3.4. Measurements

Morphologies of the as-synthesized AuPt NPCs@MWCNTs and Pt NPs@MWCNTs nanocomposites were measured by SEM (Hitachi S4800, Tokyo, Japan) and TEM (JEOL2011, Tokyo, Japan) measurements. Power XRD measurement was performed on a Shimadzu XRD-6000 (Kyoto,

Japan) using Cu Kα radiation (1.5406 Å) of 40 kV and 20 mA. For the XPS analysis, a VG Scientific ESCALab220i-XL electron spectrometer (East Grinstead, UK) was used to confirm the valence state of the elements, which used Al Kα (1486.6 eV) as X-ray and a C1s peak (284.8 eV) as the internal reference. The base pressure was approximately 3×10^{-9} mbar.

All The electrochemical experiments reported here were carried out at CHI705A (CH Instruments, Shanghai, China) electrochemical workstation. In the electrochemical measurement of methanol oxidation, a three-electrode system was employed, with AuPt NPCs@MWCNTs or Pt NPs@MWCNTs as the working electrode, Ag/AgCl as the reference electrode, and a platinum wire as the counter electrode. All the experiments reported here were carried out at ambient temperature.

4. Conclusions

AuPt NPCs@MWCNTs with a high electrochemical active surface area were successfully prepared by electrochemical methods. The introduction of the Au component effectively prevented the catalysts from carbonaceous intermediate poisoning. The AuPt NPCs@MWCNTs nanocomposite significantly improved the forward oxidation peak current of the methanol oxidation reaction in the application of direct methanol fuel cells. The ratio of the forward oxidation peak current and reverse oxidation peak current (I_f/I_b = 2.4) was much higher than the Pt NPs@MWCNTs sample (I_f/I_b = 1.7). The synthetic strategy of AuPt NPCs@MWCNTs directly facilitated other platinum-based nanocomposites, which have great potential as photocatalysts and electrocatalysts.

References

1. Aricò, A.S.; Srinivasan, S.; Antonucci, V. DMFCs: From fundamental aspects to technology development. *Fuel Cells* **2015**, *1*, 133–161. [CrossRef]
2. Jiang, Z.J.; Jiang, Z.; Tian, X.N.; Luo, L.; Liu, M. Sulfonated holey graphene oxide (SHGO) filled Sulfonated Poly(Ether Ether Ketone) membrane: The role of holes in the SHGO in improving its performance as proton exchange membrane for direct methanol fuel cells. *ACS. Appl. Mater. Interfaces* **2017**, *9*, 20046–20056. [CrossRef] [PubMed]
3. Kumar, G.G.; Manthiram, A. Sulfonated polyether ether ketone/strontium zirconite@TiO₂ nanocomposite membranes for direct methanol fuel cells. *J. Mater. Chem. A* **2017**, *5*, 20497–20504. [CrossRef]
4. Li, K.; Jin, Z.; Ge, J.; Xing, W. Platinum nanoparticles partially-embedded into carbon sphere surfaces: A low metal-loading anode catalyst with superior performance for direct methanol fuel cells. *J. Mater. Chem. A* **2017**, *5*, 19857–19865. [CrossRef]
5. Zhao, X.; Yin, M.; Ma, L. Recent advances in catalysts for direct methanol fuel cells. *Energy Environ. Sci* **2011**, *4*, 2736–2750. [CrossRef]
6. Li, Q.; Wang, T.; Havas, D.; Zhang, H.; Xu, P.; Han, J.; Cho, J.; Wu, G. High-performance direct methanol fuel cells with precious-metal-free cathode. *Adv. Sci.* **2016**, *3*, 1600140. [CrossRef] [PubMed]
7. Mallick, R.K.; Thombre, S.B.; Shrivastava, N.K. Vapor feed direct methanol fuel cells (DMFCs): A review. *Renew. Sustain. Energy Rev.* **2016**, *56*, 51–74. [CrossRef]
8. Li, X.; Faghri, A. Review and advances of direct methanol fuel cells (DMFCs) part I: Design, fabrication, and testing with high concentration methanol solutions. *J. Power Sources* **2013**, *226*, 223–240. [CrossRef]
9. Jang, S.; Kim, S.; Sang, M.K.; Choi, J.; Yeon, J.; Bang, K.; Ahn, C.; Hwang, W.; Her, M.; Cho, Y.H.; et al. Interface engineering for high-performance direct methanol fuel cells using multiscale patterned membranes and guided metal cracked layers. *Nano Energy* **2017**, *43*, 149–158. [CrossRef]

10. Shu, C.; Song, B.; Wei, X. Mesoporous 3D nitrogen-doped yolk-shelled carbon spheres for direct methanol fuel cells with polymer fiber membranes. *Carbon* **2018**, *129*, 613–620. [CrossRef]
11. Huang, H.; Zhu, J.; Li, D. Pt nanoparticles grown on 3D RuO_2-modified graphene architectures for highly efficient methanol oxidation. *J. Mater. Chem. A* **2017**, *5*, 4560–4567. [CrossRef]
12. Mcnicol, B.D.; Rand, D.A.J.; Williams, K.R. Direct methanol–air fuel cells for road transportation. *J. Power Sources* **1999**, *83*, 15–31. [CrossRef]
13. Bashyam, R.; Zelenay, P. A class of non-precious metal composite catalysts for fuel cells. *Nature* **2006**, *443*, 63–66. [CrossRef] [PubMed]
14. Jarvi, T.D.; Sriramulu, A.; Stuve, E.M. Potential dependence of the yield of carbon dioxide from electrocatalytic oxidation of methanol on platinum (100). *J. Phys. Chem.* **1997**, *101*, 3649–3652. [CrossRef]
15. Jones, D.J.; Rozière, J.; Marrony, M. High-temperature DMFC stack operating with non-fluorinated membranes. *Fuel Cells Bull.* **2005**, *2005*, 12–15. [CrossRef]
16. Ren, X.; Zelenay, P.; Thomas, S. Recent advances in direct methanol fuel cells at los alamos national laboratory. *J. Power Sources* **2000**, *86*, 111–116. [CrossRef]
17. Bu, L.; Zhang, N.; Guo, S. Biaxially strained PtPb/Pt core/shell nanoplate boosts oxygen reduction catalysis. *Science* **2016**, *354*, 1410–1414. [CrossRef] [PubMed]
18. Gurau, B.; Smotkin, E.S. Methanol crossover in direct methanol fuel cells: A link between power and energy density. *J. Power Sources* **2002**, *112*, 339–352. [CrossRef]
19. Huang, H.; Wang, X. Recent progress on carbon-based support materials for electrocatalysts of direct methanol fuel cells. *J. Mater. Chem. A* **2014**, *2*, 6266–6291. [CrossRef]
20. Seiler, T.; Savinova, E.R.; Friedrich, K.A. Poisoning of PtRu/C catalysts in the anode of a direct methanol fuel cell: A DEMS study. *Electrochim. Acta* **2004**, *49*, 3927–3936. [CrossRef]
21. Wang, C.Z.; Zhang, Y.; Zhang, Y.J.; Xu, P.; Feng, C.M.; Chen, T.; Guo, T.; Yang, F.N.; Wang, Q.; Wang, J.X.; et al. Highly Ordered Hierarchical Pt and PtNi Nanowire Arrays for Enhanced Electrocatalytic Activity towards Methanol Oxidation. *ACS Appl. Mater. Interfaces* **2018**, *10*, 9444–9450. [CrossRef] [PubMed]
22. Antolini, E.; Salgado, J.R.C.; Gonzalez, E.R. The methanol oxidation reaction on platinum alloys with the first row transition metals: The case of Pt–Co and –Ni alloy electrocatalysts for DMFCs: A short review. *Appl. Catal. B-Environ.* **2006**, *63*, 137–149. [CrossRef]
23. Drillet, J.F.; Ee, A.; Friedemann, J. Oxygen reduction at Pt and Pt70Ni30 in H_2SO_4/CH_3OH solution. *Electrochim. Acta* **2002**, *47*, 1983–1988. [CrossRef]
24. Ordóñez, L.C.; Escobar, B.; Barbosa, R. Enhanced performance of direct ethanol fuel cell using Pt/MWCNTs as anodic electrocatalyst. *J. Appl. Electrochem.* **2015**, *45*, 1205–1210. [CrossRef]
25. Wang, S.; Jiang, S.P.; White, T.J. Synthesis of Pt and Pd nanosheaths on multi-walled carbon nanotubes as potential electrocatalysts of low temperature fuel cells. *Electrochim. Acta* **2010**, *55*, 7652–7658. [CrossRef]
26. Prabhuram, J.; Zhao, T.S.; Liang, Z.X. A simple method for the synthesis of PtRu nanoparticles on the multi-walled carbon nanotube for the anode of a DMFC. *Electrochim. Acta* **2007**, *52*, 2649–2656. [CrossRef]
27. Hwang, C.B.; Fu, Y.S.; Lu, Y.L. Synthesis, characterization, and highly efficient catalytic reactivity of suspended palladium nanoparticles. *J. Catal.* **2000**, *195*, 336–341. [CrossRef]
28. Schmid, G. Large metal clusters and colloids-metals in the embryonic state. *Chem. Rev.* **1998**, *92*, 1709–1727. [CrossRef]
29. Treboux, G.; Paul Lapstun, A.; Silverbrook, K. An intrinsic carbon nanotube heterojunction diode. *J. Phys. Chem. B* **1999**, *103*, 1871–1875. [CrossRef]
30. Kabbabi, A.; Gloaguen, F.; Andolfatto, F. Particle-size effect for oxygen reduction and methanol oxidation on Pt/C inside a proton-exchange membrane. *J. Electroanal. Chem.* **1994**, *373*, 251–254. [CrossRef]
31. Haruta, M.; Date, M. ChemInform abstract: Advances in the catalysis of Au nanoparticles. *Cheminform* **2010**, *33*. [CrossRef]
32. Valden, M.; Lai, X.; Goodman, D.W. Onset of catalytic activity of gold clusters on titania with the appearance of nonmetallic properties. *Science* **1998**, *281*, 1647–1650. [CrossRef] [PubMed]
33. Xu, C.; Su, J.; Xu, X. Low temperature CO oxidation over unsupported nanoporous gold. *J. Am. Chem. Soc.* **2016**, *129*, 42–43. [CrossRef] [PubMed]
34. Gopalan, A.I.; Lee, K.P.; Manesh, K.M. Gold nanoparticles dispersed into poly(aminothiophenol) as a novel electrocatalyst—Fabrication of modified electrode and evaluation of electrocatalytic activities for dioxygen reduction. *J. Mol. Catal. A Chem.* **2006**, *256*, 335–345. [CrossRef]

35. Guo, S.; Fang, Y.; Dong, S.J. High-efficiency and low-cost hybrid nanomaterial as enhancing electrocatalyst: Spongelike Au/Pt core/shell nanomaterial with hollow cavity. *J. Phys. Chem. C* **2007**, *111*, 17104–17109. [CrossRef]

36. Baglio, V.; Stassi, A.; Blasi, A.D. Investigation of bimetallic Pt–M/C as DMFC cathode catalysts. *Electrochim. Acta* **2008**, *53*, 1360–1364. [CrossRef]

37. Luo, J.; Njoki, P.N.; Lin, Y. Characterization of carbon-supported AuPt nanoparticles for electrocatalytic methanol oxidation reaction. *Langmuir* **2006**, *22*, 2892–2898. [CrossRef] [PubMed]

38. Zeng, J.; Yang, J.; Lee, J.Y. Preparation of carbon-supported core−shell Au−Pt nanoparticles for methanol oxidation reaction: The promotional effect of the Au Core. *J. Phys. Chem. B* **2006**, *110*, 24606–24611. [CrossRef] [PubMed]

39. Banerjee, I.; Kumaran, V.; Santhanam, V. Synthesis and characterization of Au@Pt nanoparticles with ultrathin platinum overlayers. *J. Phys. Chem. C* **2015**, *119*, 5982–5987. [CrossRef]

40. Yang, Z.; Yang, X.N.; Xu, Z. Molecular Dynamics Simulation of the Melting Behavior of Pt−Au Nanoparticles with Core−Shell Structure. *J. Phys. Chem. C* **2017**, *112*, 4937–4947. [CrossRef]

41. Yang, K.; Xiao, C.; Guan, J. Nickel silicides prepared from organometallic polymer as efficient catalyst towards hydrogenation of phenylacetylene. *Catal. Today* **2015**, *246*, 176–183. [CrossRef]

42. Salernitano, E.; Giorgi, L.; Makris, T.D. Direct growth of carbon nanofibers on carbon-based substrates as integrated gas diffusion and catalyst layer for polymer electrolyte fuel cells. *Int. J. Hydrogen Energy* **2014**, *39*, 15005–15016. [CrossRef]

43. Liu, J.; Li, X.; Dai, L. Water-assisted growth of aligned carbon nanotube–ZnO heterojunction arrays. *Adv. Mater.* **2010**, *18*, 1740–1744. [CrossRef]

44. Xu, J.; Zhao, T.; Liang, Z. Facile preparation of AuPt alloy nanoparticles from organometallic complex precursor. *Chem. Mater.* **2008**, *20*, 1688–1690. [CrossRef]

45. Søgaard, M.; Odgaard, M.; Skou, E.M. An improved method for the determination of the electrochemical active area of porous composite platinum electrodes. *Solid State Ion.* **2017**, *145*, 31–35. [CrossRef]

46. Nouralishahi, A.; Rashidi, A.M.; Mortazavi, Y. Enhanced methanol electro-oxidation reaction on Pt-CoO$_x$/MWCNTs hybrid electro-catalyst. *Appl. Surf. Sci.* **2015**, *335*, 55–64. [CrossRef]